Construction and Building Materials 347 (2022) 128565

Contents lists available at ScienceDirect

Construction and Building Materials

journal homepage: www.elsevier.com/locate/conbuildmat

FEM and experimental investigations of concrete temperature field in the massive stemwall of the bridge abutment

Aleksandra Kuryłowicz-Cudowska *, Krzysztof Wilde

Department of Mechanic of Materials and Structures, Faculty of Civil and Environmental Engineering, Gdańsk University of Technology, Narutowicza 11/12, 80-233 Gdańsk, Poland

ARTICLE INFO

Keywords:
Cast-in-place concrete
Temperature field
1-wire digital sensor
Massive structure
Abutment stemwall
Numerical simulations
Bridge

ABSTRACT

The paper deals with the prediction of early-age concrete temperature of cast-in-place stemwall of the bridge abutment. The considered object is an arch bridge located in Gdańsk. In the case of massive structures, it is particularly important to not exceed the temperature difference between the core and the concrete surface. Too high temperature gradient generates an increase in thermal stresses, what could be the reason of exceeding the tensile strength and as a consequence cracking occurrence. Therefore, the numerical simulations of concrete hardening were conducted using own codes of finite difference and finite elements method. Based on numerical results the project of monitoring system was developed. The concrete temperature of stemwall was registered during 12 days by using fifteen 1-wire digital sensors. The recorded thermal data are highly consistent with FE results, which confirms the accuracy of the finite element model. The conducted calculations and in-situ measurements allowed to determine guidelines for proper curing of massive abutment's wall.

1. Introduction

The thermal effects in young concrete are investigated by many research teams [1–6]. The first measuring equipment to detect temperatures, deformations and cracks was implemented during the construction of dams. Monitoring of concrete elements at the early stages of building process is a practical source of knowledge about the advancement of the hydration process and provides a potential tool for rationalization of the construction works. The prediction of concrete temperature fields in concrete members allows the implementation of proper care of young concrete. In the case of massive structures, it is particularly important to avoid exceeding the temperature difference between the interior and the surface layers. Too high temperature gradient generates an increase in thermal stresses, which leads to exceeding the tensile strength of the concrete and finally causes the occurrence of undesirable cracks. Smolana et al., [7,8] reported and discussed a few analytic and numerical methods for the assessment of the early age cracking risk. The prediction of the temperature fields and appropriate protective activities may affect the serviceability and durability of the concrete structure. Pipe cooling systems are one of the potentially effective measures to control the temperature of mass concrete. Huang et al., [9] showed that the pipe cooling method is an effective way to reduce both the hydration temperature and thermal stress. However, the cooling pipes are mounted in concrete permanently, despite the fact that they are truly needed during the first weeks of curing. Kheradmand et al., [10] proposed a final prototype to use cooling pipes that can be removed after structural setting of concrete, without causing any visible damage. The good way to maintain low temperature in mass elements is also proper concrete composition. The amount of Porland cement can be minimized and substituted by fly ash or slag. These supplementary cementitious materials hydrate more slowly and generate less heat than Portland cement. Another strategy is to minimize the amount of cement paste by optimizing the aggregate grading or the use of basalt aggregate which has the ability to accumulate thermal energy. In order to reduce the maximum concrete temperature and the initial rate of hydration, it is also recommended to use the lower placement temperature.

The application of numerical simulations provides a lot of technological information to recognise temperature fields at the project stage. The theoretical model of concrete hardening makes it possible to identify critical places in the volume of the structure, indicating where the proper care of concrete should be carried out, and also allows to select the location of reliable measuring points for monitoring temperature changes during the setting and hardening of cast-in-place concrete. In

* Corresponding author.
E-mail address: aleksandra.kurylowicz-cudowska@pg.edu.pl (A. Kuryłowicz-Cudowska).

https://doi.org/10.1016/j.conbuildmat.2022.128565
Received 25 April 2022; Received in revised form 12 July 2022; Accepted 22 July 2022

this study, the own measurement system working on digital 1-wire temperature sensors was applied. The development in electronics technology gives the possibility to use novel types of sensors to monitor structures during construction process. Yehia et al., [11] proved that fiber-optic sensors show capabilities to record responses of the concrete samples, due to loading or during hydration and shrinkage. Pan et al., [12] proposed a reconstruction method based on a convolutional neural network for the temperature field in dams. Zhang et al., [13] described the nondestructive monitoring of the cement hydration process by the electrochemical impedance spectroscopy. The authors reported that the hydration degree and the compressive strength have a positive correlation with the resistance parameter and the proposed model can trace and characterize the development stages of the hydration process nondestructively.

Currently, the registration of thermal changes during concrete curing is not only intended to provide information on significant temperature gradients. The maps of the concrete temperature distribution in time and space domain with the conjunction of maturity method equations allows the prediction of compressive strength of cast-in-place concrete. Especially for medium-heavy elements, the time to reach required strength is important, for example to start the prestressing process [14–17].

In literature, there are a lot of studies conducted in laboratory condition with small samples prepared by using different types of cement, aggregate or additives [18–21]. However, mentioned tests do not correspond to real structures, so the advantage of this research is the application of theoretical assumptions to the actual engineering structure. As part of the road bridge investment, the concrete temperature measurements of massive abutment stemwall were carried out. This paper presents the results of in-situ measurements and numerical analysis of temperature distribution in concrete, C30/37 class. The thermo-chemical model of concrete hardening [22] was implemented in the authors' program by using finite difference (FD) and finite element (FE) method. The results of numerical calculations were compared with the data obtained during construction works. Recommendations regarding the measurement system and maintenance of massive walls of bridge abutments were also formulated.

2. Theoretical background

2.1. Thermodynamics of concrete hydration

The process of concrete hardening is an exothermic reaction, where the main thermal effect is related to the hydration of the cement components. The amount of heat released depends on the type and content of the binder. In the case of ordinary portland cement, during hydration of 1 g of cement releases from 290 to 500 J of heat. The blast furnace slag cement is characterized by lower total heat of hydration that varies from 210 to 330 J/g.

As a result of concrete hardening, the heat exchange between the core and the environment generates a heterogeneous temperature field. For modelling non-stationary and non-linear temperature fields, the partial differential equation is required:

$$\nabla\cdot(\lambda\,\nabla T)+q_c=\rho\,c\,\dot{T} \tag{1}$$

where the basic parameters are: thermal conductivity λ (W/(m·K)), volumetric heat generation rate q_c(J/m^3), specific mass ρ (kg/m^3), and specific heat of the material c (kJ/(kg·K)). The initial condition can be assumed by the initial temperature of the concrete mix, T_0 (^{o}C). Due to the fact that the conductivity of concrete is relatively low, the temperature of the concrete core increases significantly in comparison to concrete surface. The time needed to achieve thermal equilibrium highly depends on the thickness of the element. The energy balance between the environment and the concrete surface can be expressed by Newton's (convection) [23] or Stefan-Boltzmann's (radiation) condition. Irrespective of the driving force for air movement, the heat flow from the element surface may be described using Newton's law:

$$q_0=\alpha\,(T_{surf}-T_{env}) \tag{2}$$

where α (W/(m^2·K)) means the heat transfer coefficient, and T_{surf} (^{o}C) and T_{env} (^{o}C) are the concrete surface and ambient temperatures, respectively. The numerical calculations intended to supplement for real concrete member must be as simple as possible because the information about temperature differences must be available in real time, to apply proper care of young concrete. Hence, the authors states that a thermo-chemo-hygro-mechanical model proposed by Di Luzio – Cusatis's [24] would be too complex for in situ applications. Finally, the conception suggested by Cervera et al., [22] has been implemented. This approach omits the heat movement of migrating moisture, what is consistent with many authors [25,26], and it assumes that the heat transport is executed only through conduction.

Cervera's model is based on coupled equations: the thermal equilibrium and the chemical kinetics equation defined as a function of the development of the hydration degree:

$$\nabla\cdot\lambda\nabla T+Q_\xi\dot{\xi}=\rho c\dot{T} \tag{3}$$

$$\dot{\xi}=\widetilde{A}\,(\xi)\;\exp\left(-\frac{\mathrm{E_a}}{\mathrm{R\;T}}\right) \tag{4}$$

The phenomenon of heat transfer is controlled by many parameters:ρ,c,λ, material constant Q_ξ (J/m^3) (heat of cement hydration in concrete), gas constant R (J/(mol·K)), and activation energy E_a (J/mol). The rate of the heat of hydration varies during maturation and after the initial rise to the maximum value gradually decreases. The mechanical properties of concrete changing in time and the dominant mechanism of hydration of cement is the formation of new hydrates. Thus, normalized internal variable i.e. the hydration degree ξ (-) for the prediction of the advancement of the hardening process, was introduced. The rate of the internal heat source q_c is described by the formula: $Q_\xi\dot{\xi}$ and a pronounced relationship ξ on temperature T is observed. The formulation of hydration progress $\widetilde{A}\,(\xi)$ is expressed as the product of the chemical affinity and permeability, thus, the rate of hydration is given by:

$$\dot{\xi}=\underbrace{\frac{\kappa}{n_0}\left(\frac{A_0}{\kappa}\,\frac{1}{\xi_{\max}}+\xi\right)(\xi_{\max}-\xi)\exp\left(-\overline{\mathrm{n}}\,\frac{\xi}{\xi_{\max}}\right)}_{\widetilde{A}(\xi)=\;\overline{A}\;\eta\;\;(normalisedchemicalaffinity)}\;\underbrace{\exp\left(-\frac{\mathrm{E_a}}{\mathrm{R\;T}}\right)}_{(Arrheniustyplaw)} \tag{5}$$

An adiabatic calorimetric test of concrete cube allows the measuring of normalised chemical affinity$\widetilde{A}\,(\xi)$. The parameters κ/n_0 (1/h), A_0/κ (-), and $\overline{n}$ (-) are adjusted using a regression analysis by fitting the function $\widetilde{A}\,(\xi)$ to the data of the calorimetric investigation [22]. Cervera's model is suitable for both, normal and high performance concrete, and its possibilities are presented by a wide range of experimental studies, including temperature measurements on desk of concrete viaduct.

2.2. One-dimensional approach for nonlinear thermal problem

Differential equation of heat conduction in concrete, proposed by Cervera [22] can be solved using the finite difference method. In the FD method, in the classical formulation of the differential equation, derivatives of functions are replaced with finite differences (difference quotients) in a discretized space. The temperature field $T(x,t)$ variable in space (m_s) and time domainn_s. For a space of length$L$, the distance between nodes is:

$$\Delta x = L/(m_s - 1) \tag{6}$$

In order to obtain a stable solution for explicit discretization, the following criterion has to be considered:

$$\Delta t \leq \frac{\rho c}{2\lambda}\left(\Delta x^2\right) \tag{7}$$

The starting value for prediction can be written as:

$$T_{n,m} = T_0 \xi_{n,m} = 0 \tag{8}$$

hence, the rate of hydration degree is given by:

$$\dot{\xi}_{n,m} = \frac{\kappa}{n_0}\left(\frac{A_0}{\kappa}\frac{1}{\xi_{\max}} + \xi_{n,m}\right)(\xi_{\max} - \xi_{n,m}) \exp\left(-\bar{n}\frac{\xi_{n,m}}{\xi_{\max}}\right) \exp\left(-\frac{E_a}{R\,T_{n,m}}\right) \tag{9}$$

Based on the above data, the starting values for iteration process are determined:

$$\xi_{n+1,m} = \xi_{n,m} + \dot{\xi}_{n,m}\,\Delta t \tag{10}$$

$$\begin{aligned} \lambda \cdot \frac{\partial^2 T}{\partial x^2} + Q_\xi \dot{\xi} &= \rho c \frac{\partial T}{\partial t}, \\ \lambda \frac{T_{n,m+1} - 2 \cdot T_{n,m} + T_{n,m-1}}{\Delta x^2} + Q_\xi \dot{\xi}_{n,m} &= \rho c \frac{T_{n+1,m} - T_{n,m}}{\Delta t}, \\ T_{n+1,m} = T_{n,m} + \frac{\lambda}{\rho c}\frac{\Delta t}{\Delta x^2}\left(T_{n,m+1} - 2\,T_{n,m} + T_{n,m-1}\right) + \frac{\Delta t}{\rho c} C\, Q_{\max}\, \dot{\xi}_{n,m}\ . \end{aligned} \tag{11}$$

Then, using the simple iteration scheme, the temperature value in the new step is determined. The iterative process ends with the convergence condition(ε) :

$$\left|T_{n+1,m}^{(i+1)} - T_{n+1,m}^{(i)}\right| / T_r < \varepsilon \tag{12}$$

where T_r is the reference temperature. The iteration results are updated to the new step, and the boundary conditions are adopted each time according to equations:

$$T_{n+1,1} = \left(\frac{\lambda_{iz}}{d_{iz}}T_{env} + \frac{\lambda}{\Delta x}T_{n+1,2}\right)/\left(\frac{\lambda_{iz}}{d_{iz}} + \frac{\lambda}{\Delta x}\right) \tag{13}$$

$$T_{n+1,m_s} = \left(\frac{\lambda_{iz}}{d_{iz}}T_{env} + \frac{\lambda}{\Delta x}T_{n+1,m_s-1}\right)/\left(\frac{\lambda_{iz}}{d_{iz}} + \frac{\lambda}{\Delta x}\right) \tag{14}$$

where λ_{iz} is the insulation coefficient of thermal conductivity and d_{iz} means the thickness of the insulation (Fig. 1). For the described model, the validation process was successfully carried out on the basis of literature data [22], and then used for the analysis of own cases of concrete temperature distribution.

2.3. Finite element method assumption

In the case of complex geometry of concrete structure, the finite element method is an appropriate way to predict concrete temperature development. The procedure of the authors' program for the numerical calculation of the initial-boundary value problem, by means of the Finite Element Method (FEM), is explained in detail in paper [14] and summarized below.

The heat transfer is described by the Fourier equation for heat conduction with internal sources:

$$\nabla\cdot(\lambda\,\nabla T) + q_c - \rho\, c\, \dot{T} = 0 \text{ on structural body B} \tag{15}$$

The boundary conditions were defined in the following form: Dirichlet condition, taking into account the known temperature distribution $\overline{T}$ on∂B_T:

$$T(x,y,z;\ t) = \overline{T}_{\partial B_T}(x,y,z;\ t) for\, t > 0\, on\, \partial B_T \tag{16}$$

and convective (Newman):

$$(-\lambda\nabla T)\cdot\boldsymbol{n} = \alpha\,(T_{surf} - T_{env}) = q_0 for\, t > 0\, on\, \partial B_q \tag{17}$$

where $\overline{T}_{\partial B_T}$ is the prescribed temperature on boundary∂B_T, T_{env} means the environmental temperature, α is the heat transfer coefficient, q_0 is the heat flux on boundary∂B_q, $-\lambda\,\nabla T = \boldsymbol{q}$ is the heat flux, and $\boldsymbol{n}$ is the unit vector pointing out of the structural body (Fig. 2**a**). Furthermore, it is assumed that the initial conditions are given by:

$$T(x,y,z,t = 0) = T_0(x,y,z)\, on\, B \tag{18}$$

Equivalent to the strong formulation (eq. to) is the functional (weak form):

$$I = \frac{1}{2}\int_B\left(\lambda\left(\frac{\partial T}{\partial x}\right)^2 + \lambda\left(\frac{\partial T}{\partial y}\right)^2 + \lambda\left(\frac{\partial T}{\partial z}\right)^2 - 2\left(q_c - \rho c\frac{\partial T}{\partial t}\right)T\right)\mathrm{dB} + \frac{1}{2}\int_{\partial B_q}\alpha\left(T_{surf} - T_{env}\right)^2 \mathrm{d}(\partial \mathrm{B_q}) \tag{19}$$

where Euler-Lagrange equations are eq. and boundary conditions, while the conditions are met directly, and they are not difficult in FEM [27,28]. Finally, the determination of the temperature field $T(x,y,z;\ t) \in$ U for $t > 0$ on $B \subset E^{nE}$ leads to the minimization of the functional with meeting the initial conditions. U stands for the space of all feasible solutions, and $n_E = 3$ is the dimension of the Euclidean space. The discretization of the defined initial-boundary problem, assuming that it meets the conditions of Galileo's space–time ($E^{n_E} \times R_+$), is divided into two phases. The first phase includes the space discretization (Fig. 2**b**) by

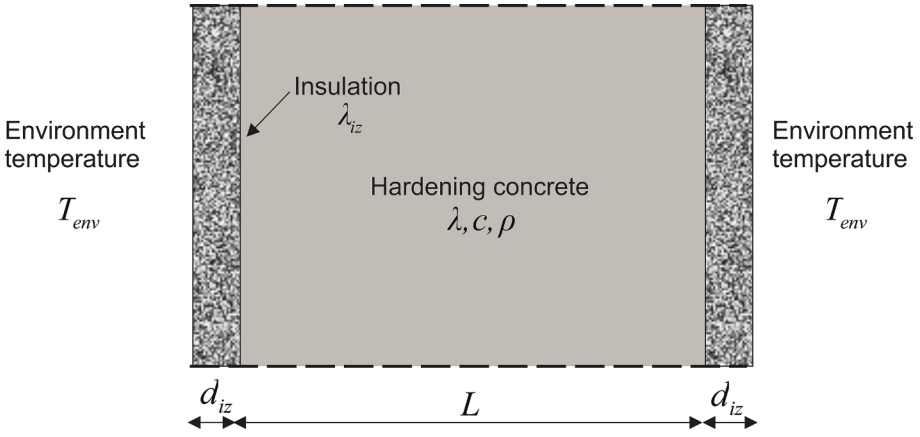

Fig. 1. The scheme of the 1D domain for the heat transfer.

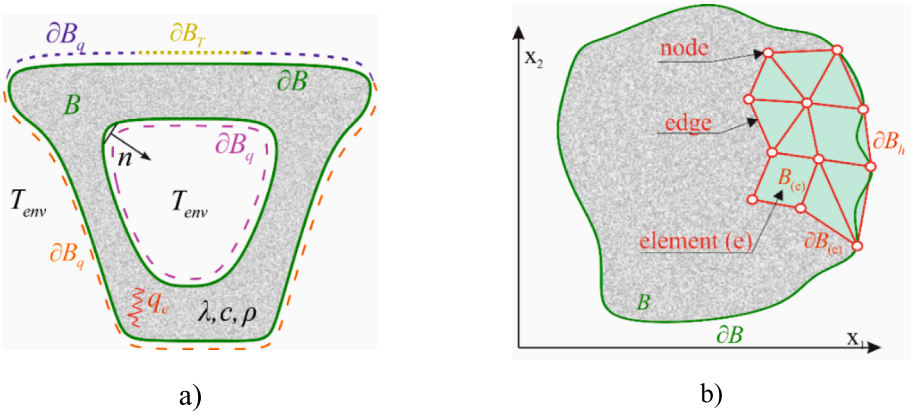

Fig. 2. a) The structural body, b) discretization.

the standard isoparametric finite elements$B \cup \partial B \subset E^{n_E}$, where $n_E = 1, 2, 3$ is the space dimension and the second phase includes the time domain discretization ($t \in R_+$) using the Euler's one-step differential forward integration scheme.

2.4. The abutment stemwall of the bridge

The considered object is an arched, single-span road bridge located in Gdańsk (Fig. 3**a**). The basic dimensions characterizing the superstructure are as follows: span length of 104.0 m, the axial spacing of the arch girders of 17.05 m, total width of 37.69 m, bicycle path width of 2.5 m, footpath width of 2.0 m, angle of intersection with an obstacle of 27.9°. The length of the analysed abutment wall is equal to 39.8 m, the wall height at the bearing level varies from 7.3 to 8.8 m and the wall thickness is 2.0 m [29]. The scope of research work included the forecasts of concrete temperature distribution, the development of a concrete temperature monitoring system, and finally in-situ measurements for abutment wall.

An abutment stemwall was made of structure concrete of C 30/37 class, using CEM I 42.5 N SR3/NA (sulphate-resistant and low-alkaline portland cement). The composition of concrete mixture and chemical properties of cement are presented in Table 1 and Table 2, respectively. The heat of cement hydration released at 72 h was equal to 315.96 J/g [30,31], Fig. 4, while in numerical calculation extrapolated value of total heat $Q_{max} = 330$ kJ/kg was assumed. A volume of 706.5 m^3 of

Table 1
Overview of mix proportions [34].

Component	(kg/m^3)
CEM I 42.5 N SR3/NA	360
Water	160
Sand 0/2	682
Granite 2/8	500
Granite 8/16	637
Plasticisers	2.70

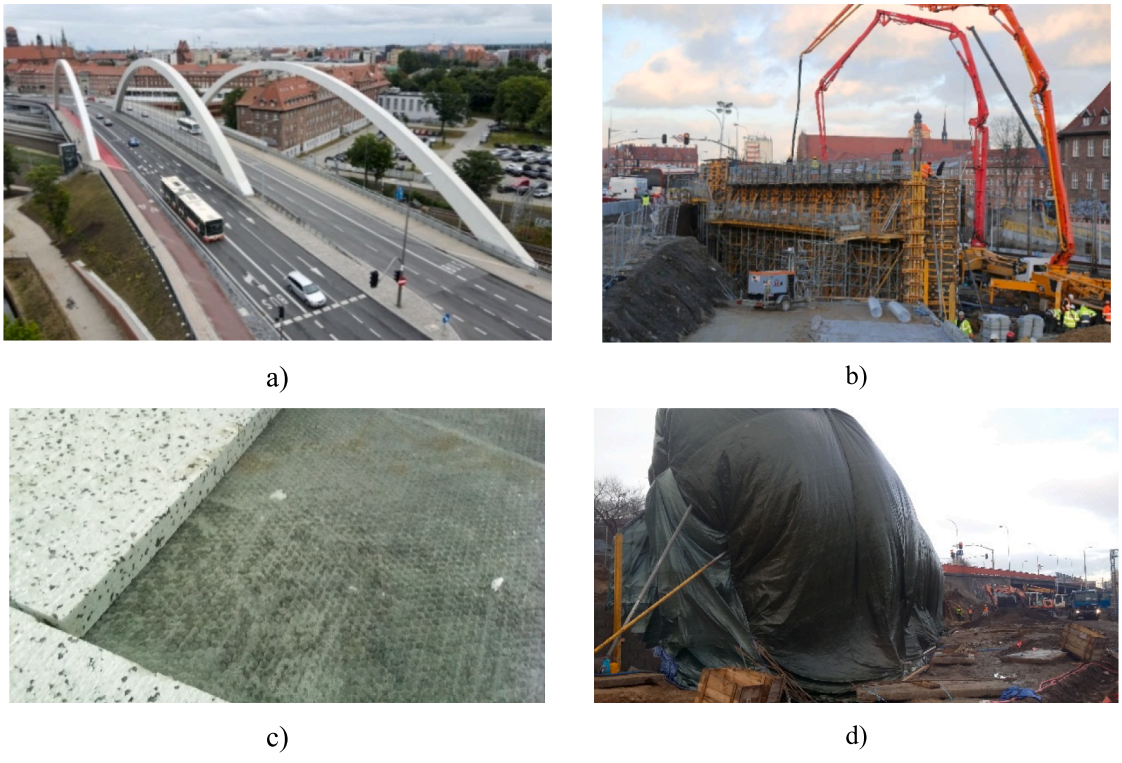

Fig. 3. a) View of the bridge opened for the public [33], b) concrete pumping, c) Styrofoam protection, d) the wall covered with tarpaulin.

Table 2
Chemical and physical properties of cement [34].

Component	CEM I 42.5 N SR3/NA
SO_3	2.23 %
Cl-	0.067 %
Na_2O	0.53 %
Al_2O_3	3.83 %
C_3A	2.22 %
$C_3AF + 2C_3A$	18.71 %
C_3S	54.21 %
Specific Blaine area	3354 cm^2/g
LOI	1.21 %

concrete was used for the considered abutment wall of the bridge. The construction process lasted from 2018 to 2020, when the bridge passed the loading tests.

The concrete works took place in December, when the average ambient temperature was about 5 °C, and the average wind speed was 4.0 m/s [32]. The wall casting lasted about 15 h, using two boom concrete pumps (Fig. 3**b**). Due to the fact that concrete was poured and placed in cold weather conditions, appropriate precautions were taken to eliminate the problems associated with low temperatures. The upper surface of the wall was protected with a 5-cm-thick Styrofoam layer to trap the heat (Fig. 3**c**). Additionally, the wall was covered with tarpaulins (Fig. 3**d**) and active heating was carried out. The frame formwork of the abutment wall was made of plywood, 2.1 cm thick.

2.5. Original measurement system

The novel temperature monitoring system was used for the field test. The device consists of a central management unit and water-proof, digital temperature sensors with a 1-wire interface (Fig. 5). The supervisory system of the equipment recognizes the sensors on the basis of unique, 16 digital serial numbers assigned to them at the production stage. The security of data exchange is ensured by CRC control, and the generator polynomial has the form of x8 + x5 + x4 + 1. The DS18B20 sensors are specified to operate in a temperature range from – 55 to + 125 °C, with an accuracy of ± 0.5 °C and does not require calibration, which guarantees the reliability of the obtained data. The device makes it possible to measure the concrete temperature at 20 points working on battery for approximately 30 days and sends data to the server every hour by a GSM modem. The measurement points can be assembled separately or by using a prefabricated bar with a number of detectors

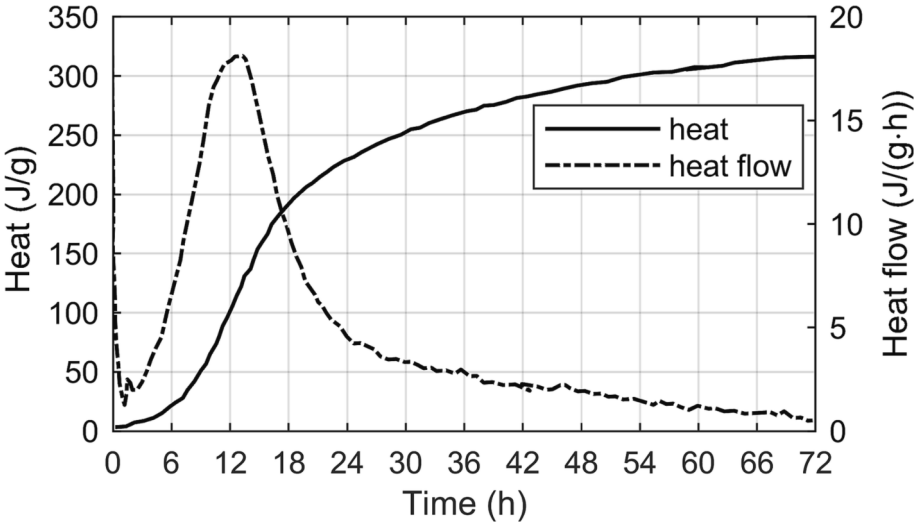

Fig. 4. Heat of hydration and heat flow of cement [30,31].

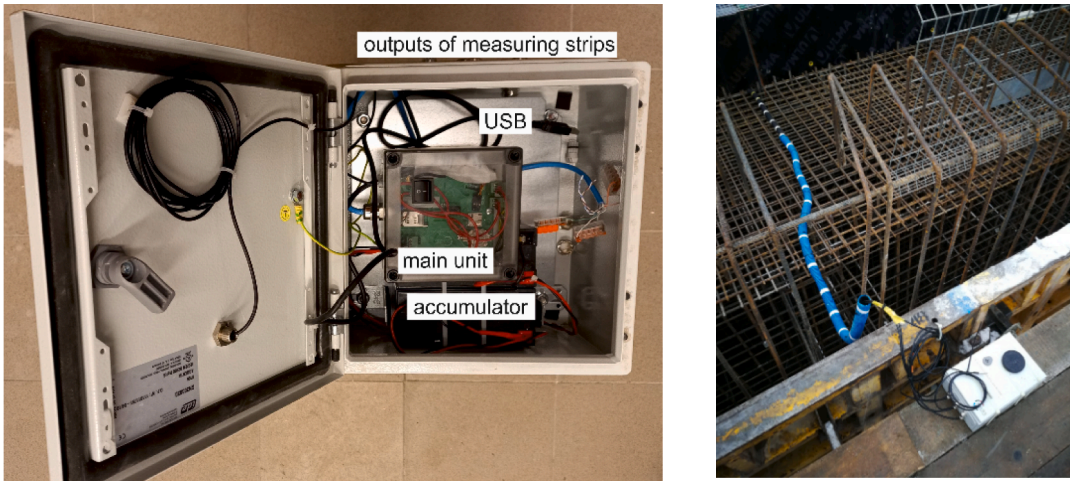

Fig. 5. a) Temperature measurement system, b) the applied system at the construction site.

arranged according to a previously prepared project.

2.6. In-situ measurements

The concrete temperature of the abutment wall (Fig. 6**a**) was measured for 288 h (12 days). The thermal data was registered with a time step of 15 min, which gives 1152 points of data. The monitoring of the concrete hardening was implemented for three testing sections: the first across the wall thickness (sensors number 11 – 15), the second along the wall height - in the middle of the wall (sensors number 21 – 25), the third along the wall height in the surface (sensors number 31 – 35). The concrete temperature was measured by 15 thermocouples. Additionally, one sensor was placed out of the structure to register ambient temperature. Data was sent to the server every 1 h via a GSM modem and were downloaded online. The locations of the thermocouples are given in Fig. 6**b**. The wall casting process is shown in Fig. 7.

Fig. 8 - Fig. 10 illustrate the registered thermal histories at all measurement locations. The ambient temperature recorded during the construction process of the abutment is also visible. The initial temperature (T_0) of the concrete mixture delivered to the construction site was equal to 11.5 °C, and the ambient temperature during concreting was about 2.0 °C. When the concrete works were completed, the wall was covered with a tarpaulin, and between 28 and 137 h the air was heated with blowers, sometimes more or less effectively (heating break from 64 h to 89 h) due to strong gusts of wind (points 36, Fig. 8 - Fig. 10). The tarpaulins were removed between 184 and 188 h, while the frame formwork was removed after finishing temperature measurements i.e. at 354 h (14 days and 18 h) of concrete hardening.

The maximum temperature of young concrete, that equals 57.0° C, was recorded in point 13 (Fig. 8), i.e. in the middle of the height and thickness of the mass structure, therefore the temperature of self-heating caused of heat of cement hydration was 45.5 °C. A temperature close to the maximum value i.e. 56.4, 56.6 and 55.6 °C was also recorded at points 22, 23, 24, respectively (Fig. 9). For points number 13 and 22, the maximum temperature appeared at the same time i.e. at 62 h from concreting of the given sensor (Fig. 8 - Fig. 9). In the case of points 23 and 24 (Fig. 9), the mentioned time was longer, due to the larger volume of embedded concrete in the upper zone of the considered abutment wall.

It can be observed that the testing points 31–35 located near the framework are more affected on ambient temperature variations (Fig. 10). The temperature time history curves at the surface layer, recorded in points 32, 33 and 34 was mutually consistent, and the maximum temperature value at these points was equal to 42.5 °C (Fig. 10). The effect of periodically insulating the upper wall surface with Styrofoam was clearly visible. The concrete temperature measured at point 25 was higher than that measured at other external points, e.g. 21, 31 or 35 (Fig. 9 - Fig. 10). Wall corners with an indication of the point no. 31, located at the junction with the foundation was particularly susceptible to cooling effect.

As demonstrated in Fig. 11, the temperature difference between the surface and the core exceeded 15 °C, from 67 to 240 h. The difference equal to 20 °C was exceeded only locally in two sections corresponding to the thermocouples 21 and 31 (max. 23.3 °C) and no. 23 and 33 (max. 22.3 °C), (Fig. 11).

The rate of temperature elevation is really rapid, while the temperature drop is more gradual and coincides with each other at most points, except points 35 and 31 due to their location. The time of reaching thermal equilibrium of the monitored wall with the ambient temperature has not been determined due to the limited period of measurements.

In the case of massive structure, the thermal–shrinkage cracks occur often in the stem of the abutment restrained by the previously cast foundation. The stresses are primarily the effect of thermal issues, because the shrinkage stresses develop slowly in the initial period of maturation and reach greater values after a longer period of hardening. When the wall is in the formwork in the cooling phase, cracks appear inside the wall. After formwork removal, due to the high surface gradients of temperature and humidity, the rapid development of surface cracks can occur. As a result, a greater range of cracks along the wall is visible.

After the formwork removal, the potential cracks in the abutment were inspected. Fig. 12 presents cracking pattern observed in stemwall (front side in red colour, backfill side in blue colour) with an indication of the distance and width of the cracks. Damages appeared in almost the same places on both sides of the wall. Mainly vertical cracks, starting at the wall–foundation interface and disappearing in the upper part of the wall, were detected. The observed damages reached from ½ to ¾ of the wall height, spaced from 1.9 to 6.0 m with width ranged between 0.1

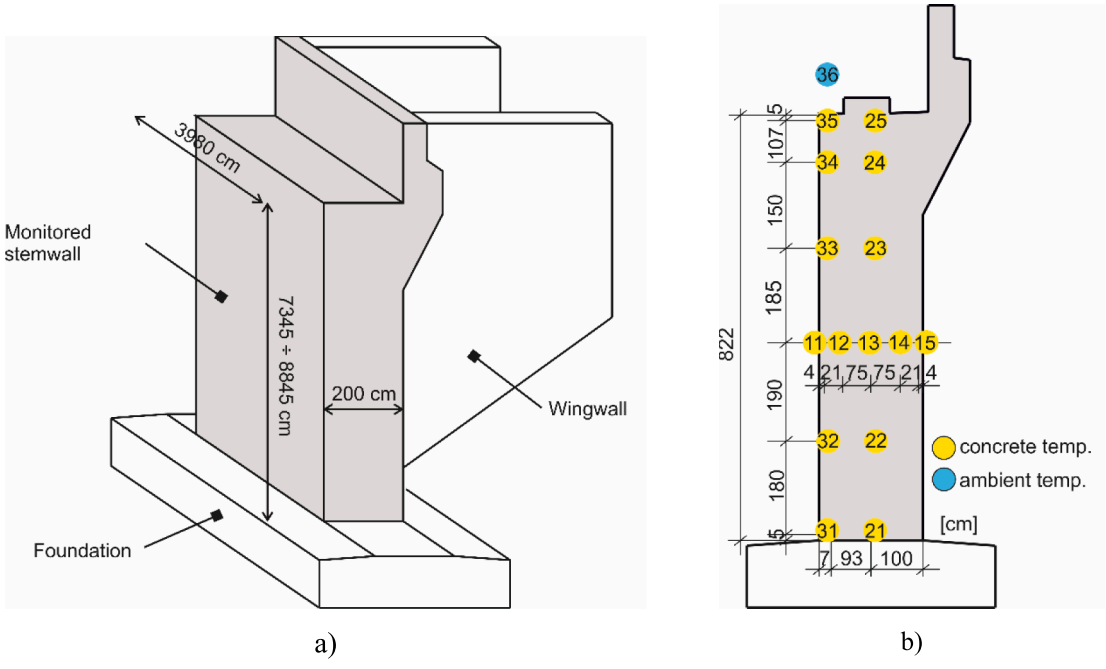

Fig. 6. a) General view of the abutment, b) locations of temperature measurement points.

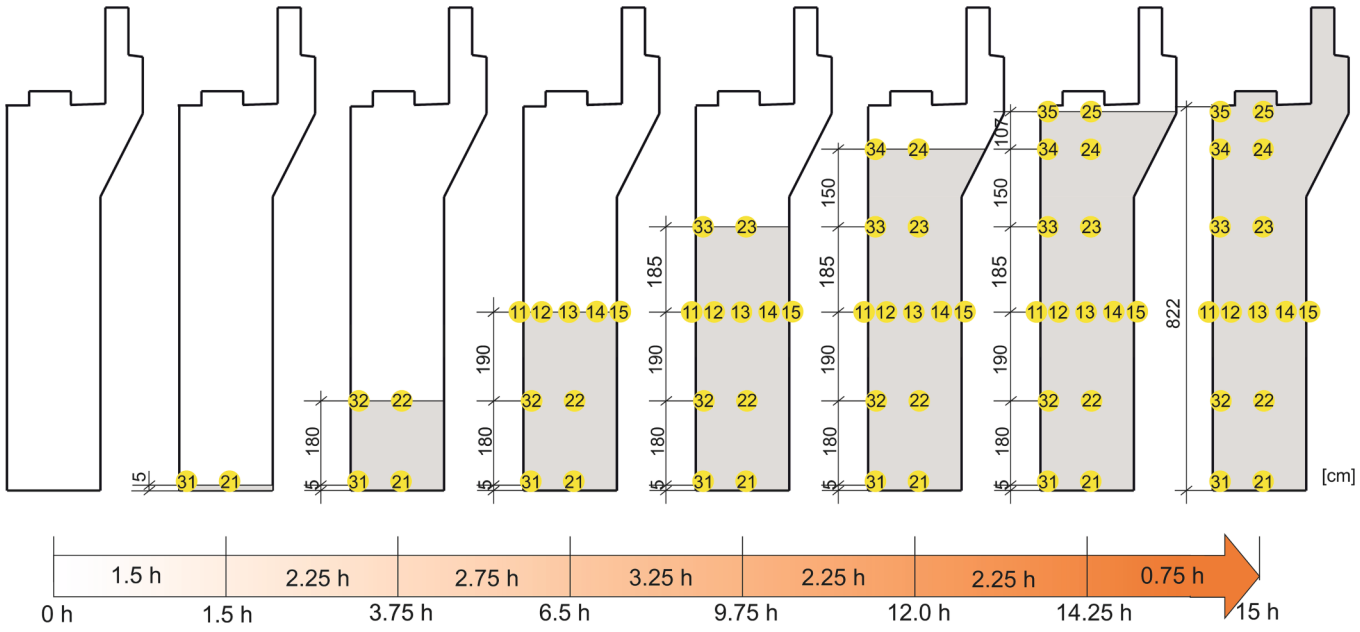

Fig. 7. Concrete casting process.

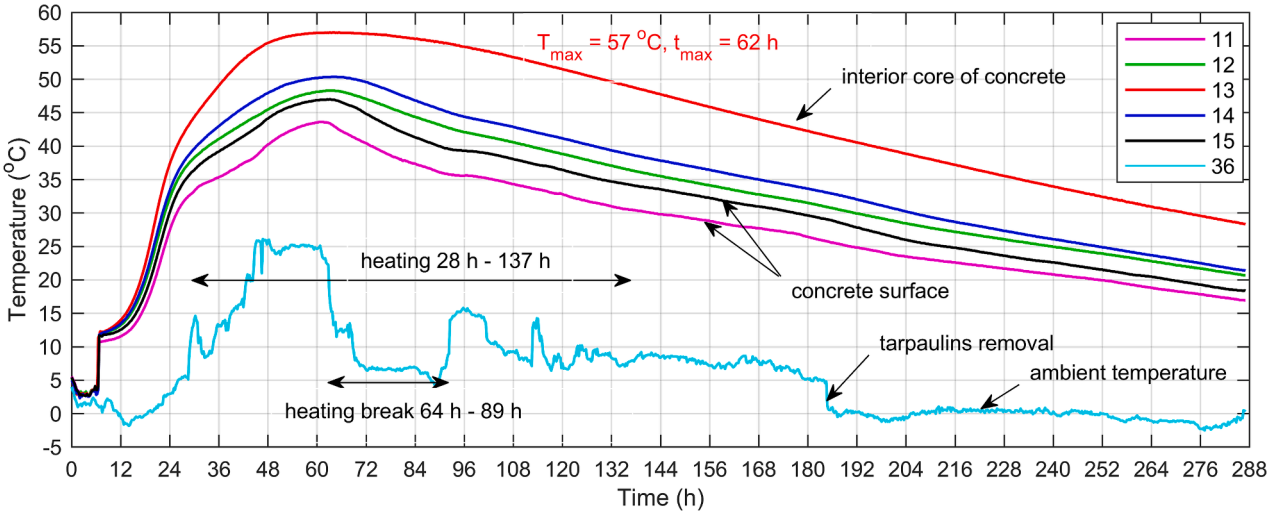

Fig. 8. Temperature evolution of concrete wall for 12 days in section no 1.

and 0.2 mm. The highest vertical cracks appeared in the centre of the wall, while near the edges, the cracks were shorter and deviated from the vertical. All cracks did not exceed the allowable cracks width 0.3 mm according to EN-1992–1-1:2008 [35]. It is worth noting that, the degree of restraint, the applied reinforcement, the temperature drop and shrinkage strains are crucial to evaluate the crack width.

3. Numerical simulations

3.1. One-dimensional calculations

Numerical calculations of temperature distribution in concrete wall were carried out using FD method in the authors' program written in the MATLAB environment. It was assumed that the wall was infinitely long and it is concreted at the same time in its entire volume. The monitored stemwall belongs to massive concrete member where setting conditions in the interior of the wall are close to adiabatic. The heat exchange between the concrete and ambient temperature occurs mainly along the thickness of the wall. One-dimensional calculations concerned the temperature distribution in 2 m- thick wall protected both sides with formwork. This case corresponded to the in-situ measurements carried out in section no. 1 (sensors 11–15).

According to Lura and Breugel [36,37] the value of specific heat of concrete c depends on the mass component per cubic meter (W) and its specific heat (cement, granite aggregate, quartz aggregate and water). For the degree of hydration $\xi = 0$, the specific heat expressed in J/(kg·K) can be written in the following form:

$$c = \frac{W_{cement}\cdot c_{cement} + W_{granite}\cdot c_{granite} + W_{quartz}\cdot c_{quartz} + W_{water}\cdot c_{water}}{W_{cement} + W_{agregate} + W_{water}} = \\ = \frac{360\cdot 825 + 1137\cdot 775 + 682\cdot 867 + 160\cdot 4187}{360 + 1137 + 682 + 160} = 1043 \quad (20)$$

The heat conduction coefficient of considered concrete λ, expressed in W/(m·K), was calculated based on thermal conductivities of the mixture components [36,37]:

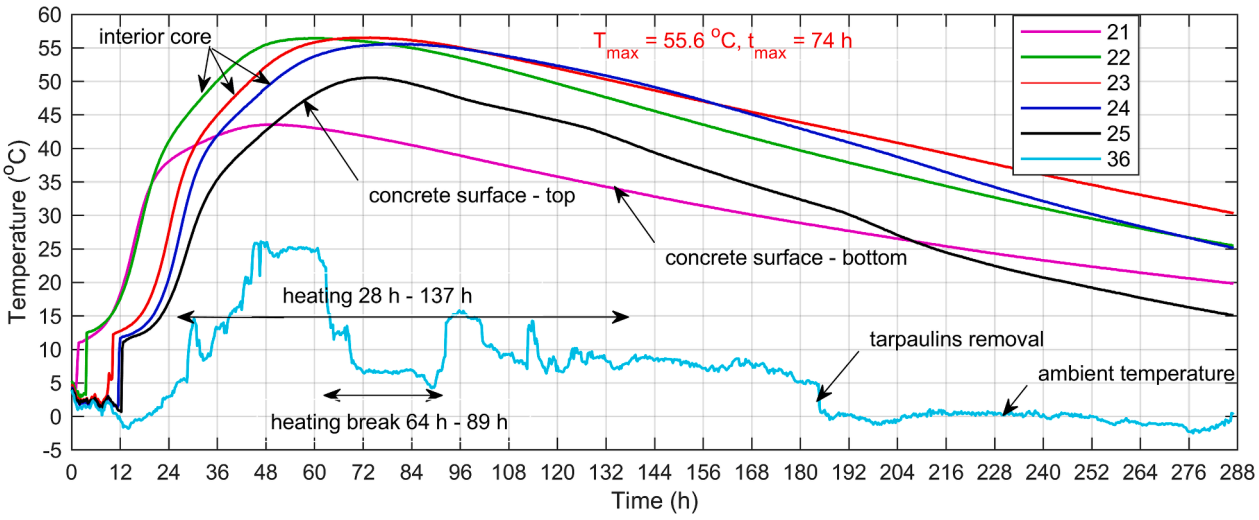

Fig. 9. Temperature evolution of concrete wall for 12 days in section no 2.

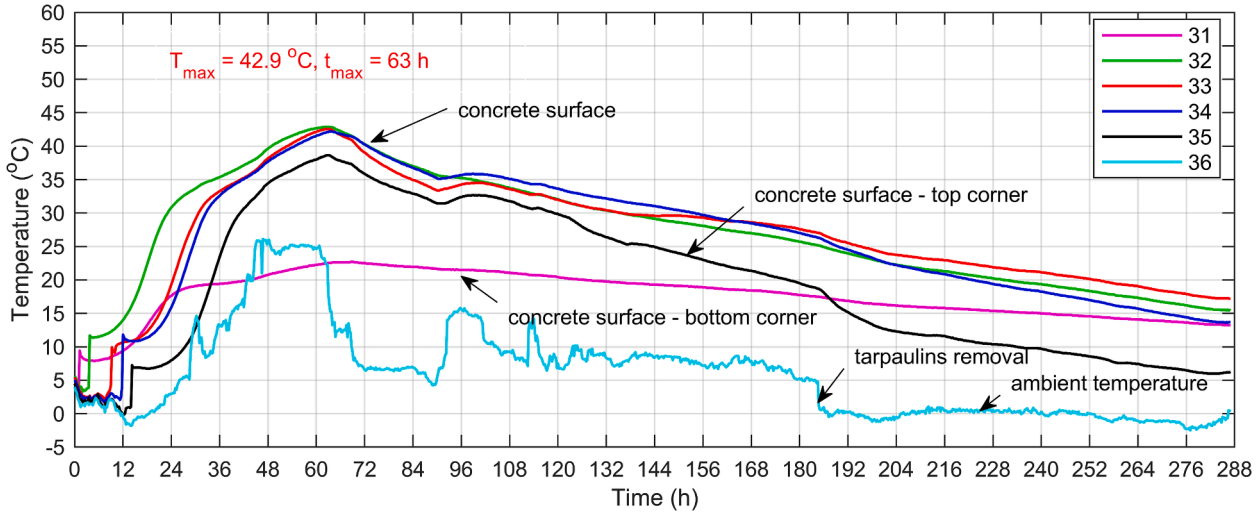

Fig. 10. Temperature evolution of concrete wall for 12 days in section no 3.

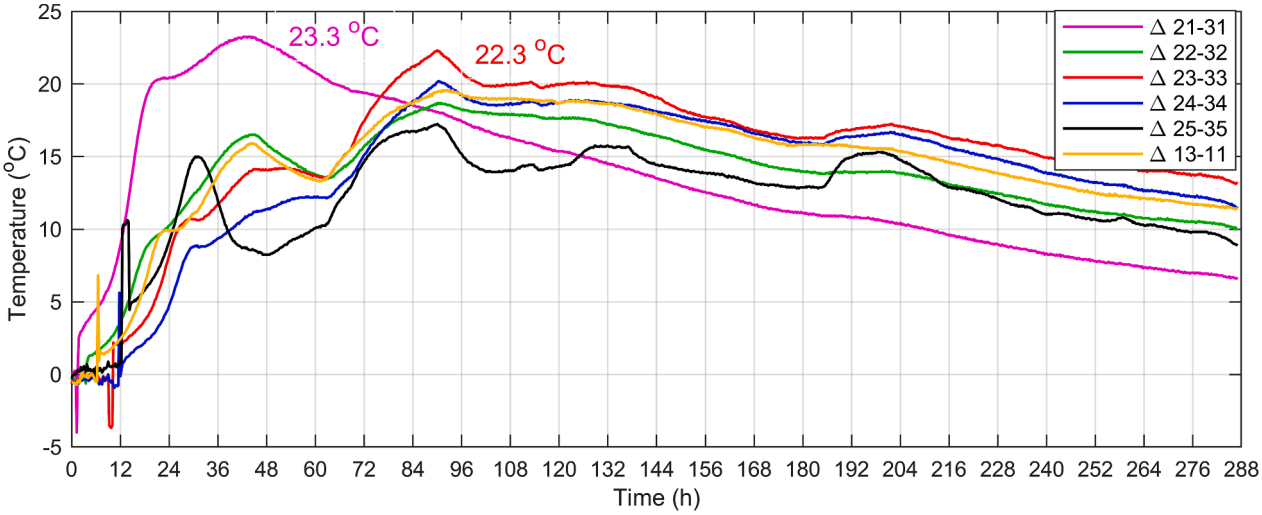

Fig. 11. The temperature difference between the core and the surface.

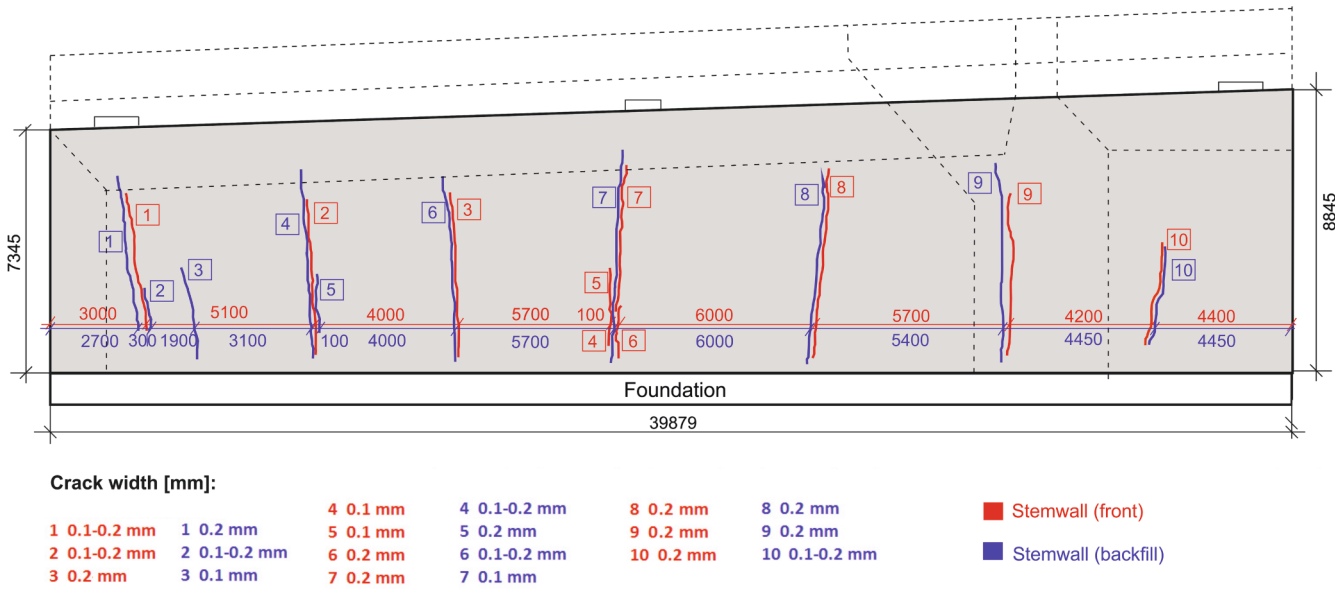

Fig. 12. The thermal cracks observed in early ages of concrete in a bridge abutment wall.

$$\lambda = \frac{W_{cement}\cdot\lambda_{cement} + W_{granite}\cdot\lambda_{granite} + W_{quartz}\cdot\lambda_{quartz} + W_{water}\cdot\lambda_{water}}{W_{cement} + W_{granit} + W_{quartz} + W_{water}} = \\ = \frac{360\cdot 1,35 + 1137\cdot 2,88 + 682\cdot 3,06 + 160\cdot 0,6}{360 + 1137 + 682 + 160} = 2,54 \quad (21)$$

The convective heat transfer coefficient on the concrete surface protected by the formwork layer was adopted using own nomograms, developed in paper [15],$\alpha_s^{form} = 3.6$ (W/(m^{2}K)). The time increment adopted in one-dimensional calculation was equal to 0.01 h. All thermophysical parameters of concrete C30/37 were assumed in accordance with Table 3 and Table 4.

The development of concrete temperature in section no 1 of massive member is shown in Fig. 13. In this case, the ambient temperature registered during the 12 days (T_{env}) was taken. The solid lines represent real measurements in points 13 – 15, while the dashed lines illustrate the results of numerical computations. Very good agreement between experimental and theoretical data for considered points was obtained. The maximum temperature value was recorded in interior core of concrete structure (point 13), while in point no 15, located in surface layer, there is a visible drop in temperature, due to heating break. After 288 h of concrete hardening the computed temperature in centre of stemwall (point 13) is about 3 °C higher than real value. Additionally, as illustrated in Fig. 14**a**, the temperature distribution in cross section of the abutment wall for selected hours was depicted. The dots correspond to the experimental data and the solid lines show calculated values. The real values of temperature in points 11 and 12 are slightly lower than computed values in every considered hour. Probably on this side of the wall the heating was less effective, due to the wind force. The map of concrete temperature in space and time domain is given in Fig. 14**b**.

3.2. FEM analysis

The finite element method is a powerful technique to represent the behaviour of the heat transfer in massive member. The own FEM software was implemented to simulate the temperature field of concrete as a function of time. In 2-dimensional model it was assumed that the stemwall was extremely long and casted at the same time in its entire volume. Initial and boundary conditions were adopted in accordance with point 4.1 i.e. wall and bottom surface protected with formwork and upper surfaces covered with Styrofoam (the insulation coefficient of thermal conductivity$\lambda^{styr} = 0.05$ (W/(mK)), thickness of Styrofoam $d^{styr} = 0.05$ m and the heat transfer coefficient $\alpha_s^{styr} = 1.0$ (W/(m^{2}K))). During the entire process of concrete curing a constant ambient temperature of 5 °C was assumed. The performed calculations did not take into account the stages of casting wall.

Table 3
Thermophysical properties of considered concrete.

C	ρ	E_a/R	w/c	ξ_{max}	Q_{max}	c	λ
(kg/m^3)	(kg/m^3)	(K)	(-)	(-)	(kJ/kg)	(kJ/(kg·K))	(W/(m·K))
360	2342	4850	0.444	1.0	330	1.043	2.54

Table 4
Model parameters.

κ/n_0	$\bar{n}$	A_0/κ	T_0	α_s^{form}
(1/h)	(-)	(-)	(°C)	(W/(m^2·K))
$1.8\cdot10^6$	2.0	$2\cdot10^{-1}$	11.5	3.6

FEM allowed the representation of a concrete continuum by discretising it into a finite number of elements. The developed model consists of 8037 nodes, 1944 9-node quadrilateral Lagrange elements and 260 3-node linear Lagrange elements. Based on careful mesh convergence criteria, an appropriate mesh size was set to be 0.10 m. The time increment adopted in FEM calculation was equal to 0.013 h. The discretization of concrete wall, and then post processing i.e. visualization of temperature distribution was carried out using the GID program.

Fig. 15 presents the results of a simulation-based on the FEM method in particular hours, with an indication of temperature range. The maps of concrete thermal fields are depicted via a color scale, where the temperature varies from 5° C to 60 °C. In the first step of calculation (0 h) the concrete temperature in entire element equals to the initial temperature$T_0 = 11.5$ °C. In the next steps the continuous temperature rise is observed and at about 60 h of curing the concrete temperature reaches the maximum value 57.2 °C. (Fig. 15). The main source of released thermal energy is located in places with the largest volume of embedded concrete. After reaching the peak, the cooling phase begins, while at 96 h the concrete temperature in abutment wall ranges from 15.9 °C to 53.5 °C. It can be seen that temperature decreases from the interior to the outer surface gradually. When the formwork was removed i. e. at 354 h, the maximum temperature was equal to 24.9 °C. After 28 days (672 h) of hardening the entire wall achieved thermal equilibrium

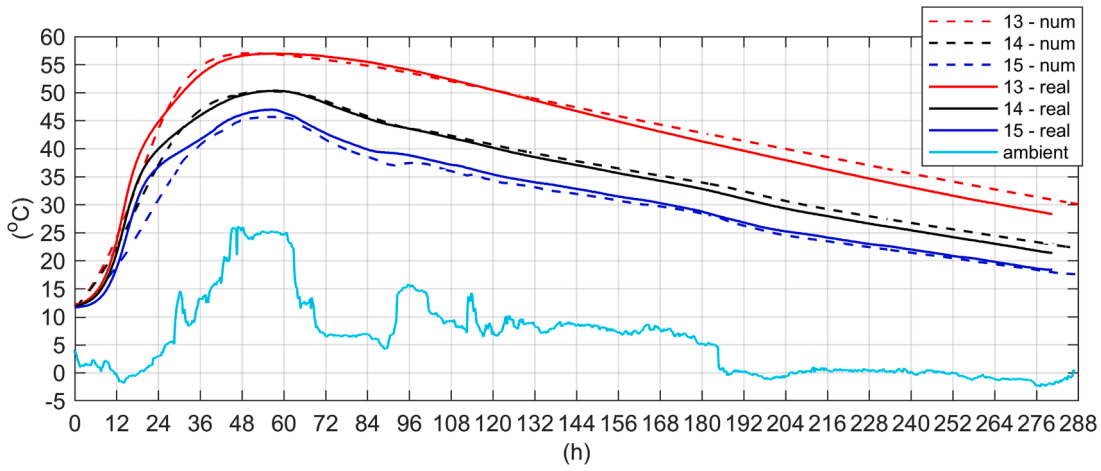

Fig. 13. Comparison of FED results and real value in section no 1.

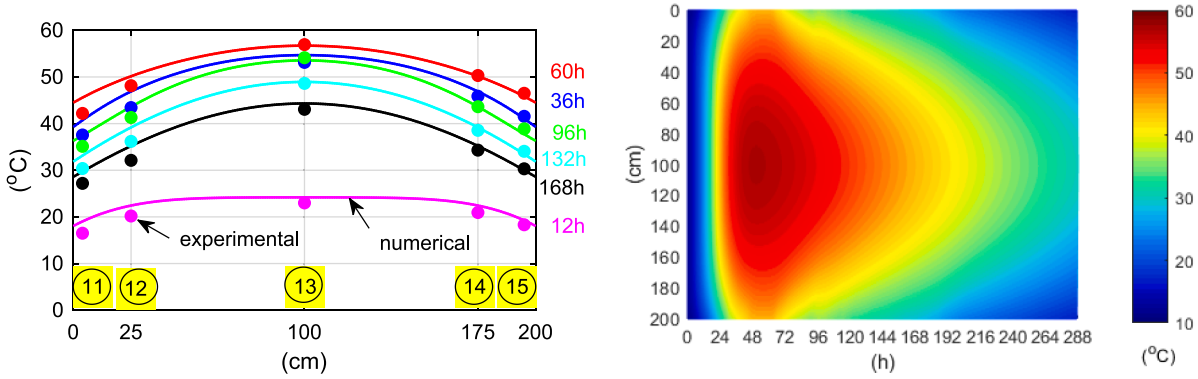

Fig. 14. The concrete temperature in section no 1: a) distribution for selected hours, b) 1D map.

with the environment, because the concrete temperature (5.1 °C ÷ 11.3 °C) was close to the ambient one.

It is worth noting that the temperature distribution strongly depends on the composition of the mixture, and above all on the weather and boundary conditions. Due to the presence of formwork installed on both sides of 2 m thick wall, except for the disturbed upper and lower parts, the stemwall is in a stabilized thermal state, corresponding to the results obtained from the one-dimensional solution. Particularly susceptible to cooling process are the upper zones of the wall with the smallest thickness. As demonstrated in Fig. 15, the influence of Styrofoam insulation on maintaining the concrete temperature at the top surface is clearly visible.

4. Discussion of results

The Portland Cement Association's (PCA) [38] proposes a simple analytical method for estimating the maximum temperature in mass concrete structure. This method evaluates the maximum temperature increase above the in-place concrete temperature, as 12 °C for every 100 kg of cement and does not provide information on the time of its occurrence. Riding [39] et al., reported that PCA formula is only applicable for concrete containing from 300 to 600 kg of cement per cubic meter and assumes that the least dimension of the concrete element equals 1.8 m. The method is dedicated to type I cement and does not provide any guidelines for considering slag cement. The PCA is suggested to calculate maximum concrete temperature T_{max} according to formula:

$$T_{\max} = T_i + \left(12\cdot\frac{W_c}{100}\right) + \left(6\cdot\frac{W_{scm}}{100}\right) = 11.5 + \left(12\cdot\frac{360}{100}\right) + \left(6\cdot\frac{0}{100}\right) = 54.7\ ^\circ C \tag{22}$$

where T_i is the initial temperature of concrete, in °C; W_c is the weight of cement, kg/m^3; and W_{scm} means the weight of supplementary cementitious materials, kg/m^3.

The actual temperature developed inside concrete cured under adiabatic conditions can also be calculated from the formulation:

$$T_{\max} = T_0 + \frac{C\cdot\xi_{\max}\cdot Q_{\max}}{c\cdot\rho} = 11.5 + \frac{360\cdot 1.0\cdot 330}{1.043\cdot 2342} = 11.5 + 48.6 = 60.1\ ^\circ C \tag{23}$$

The above maximum concrete temperatures specified by analytical and also numerical method with comparison to measured value are listed in Table 5. The highest relative error equal to 5.4 % concerns the equation (23), while the lowest error (0.4 %) is connected with FEA results. The numerically predicted adiabatic temperature rise was 57.2 °C, which is almost identical to the registered in-place temperature value of 57.0 °C. A comparison of FEA and real values difference at 90 h from the beginning of in-place casting was summarized in Table 6. In the case of numerical approach, the wall was casted at the same time in its entire volume, thus the time shift was taken into account. The biggest difference, above 20 °C, was noted for points 23–33 and 24–34, located in the zone of the highest volume of embedded concrete. The relative error of temperature difference is lower than 10 % and is higher only for

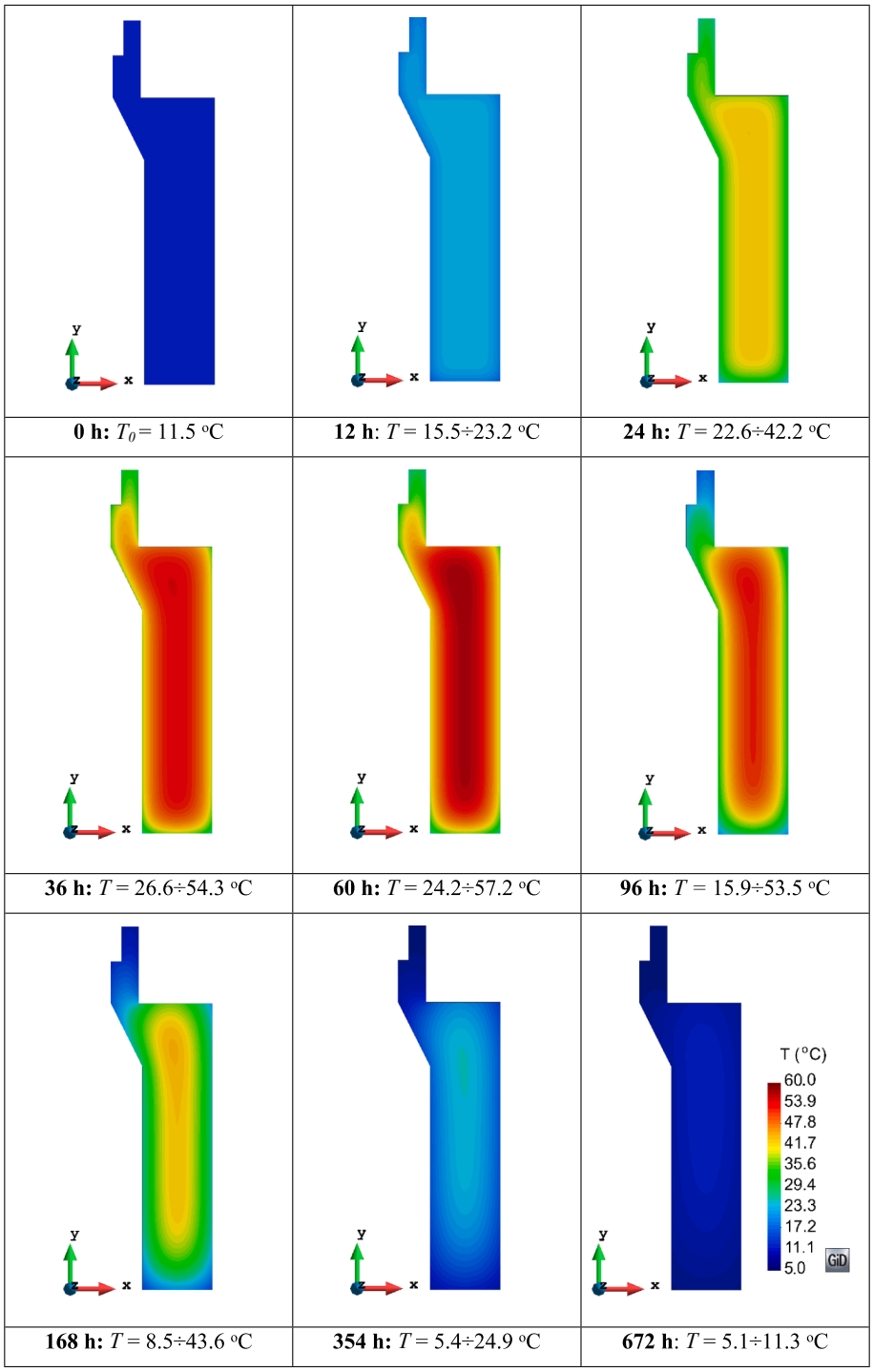

Fig. 15. The maps of concrete temperature distribution for selected hours.

Table 5
Maximum concrete temperature in the wall centre.

Calculation method	Theoretical (°C)	In-place temperature (°C)	Relative error (%)
PCA method	54.7	57.0	4.0
Equation (23)	60.1	57.0	5.4
FEM approach	57.2	57.0	0.4

Table 6
A comparison of FEM and real values temperature difference at 90 h of curing.

Sensors location	Temperature difference (°C) at 90 h FEM approach	in-place temperature	Relative error (%)
Points: 25–35	16.1	17.2	6.4
Points: 24–34	20.6	20.1	2.5
Points: 23–33	20.1	22.3	9.9
Points: 13–11	19.7	19.4	1.6
Points: 22–32	19.6	18.7	4.8
Points: 21–31	13.4	18.0	25.6

testing points 21–31. It can be affected of the specific arrangement of the point 31 at the corner of the bottom zone of the wall, where the heat can diffuse faster. By summarizing Table 5 and Table 6, it can be stated that the in-place temperature fields are consistent with the FE calculation, which confirms the accuracy of the finite element model assumptions.

5. Final remarks

The paper presents the results of numerical and experimental investigation of thermal changes caused by hydration heat in concrete stemwall of bridge abutment. The research focused on identification of temperature field in massive structure in time and space domain. The considered phenomenon is extremely important in practical engineering applications, due to the high requirements for the durability of the structure. The theoretical assumptions of the own FEM code were confirmed by using experimental measurements conducted through original temperature monitoring system. Based on the gained experiences the following findings can be drawn:

- The in-place temperature measurements show that the heating phase in concrete wall develops rapidly for the first 60 h but the generated heat is lost significantly slower. The conditions in the interior of the mass concrete element are similar to the adiabatic ones. The maximum concrete temperature equal to 57 °C appears at 62 h from the start of casting and does not exceed the limit value of 70 °C, according to EN 13,670 [40].
- The corners of the abutment wall, located at the contact zone with the foundation are particularly susceptible to cooling down, so these places require special attention. Free surfaces also need to be protected with a styrofoam or bubble wrap because the concrete has the low thermal conductivity and the temperature difference may occur between the surface and the core of structure. The proper care of external free layer reduces the risk of crack caused by thermal stresses.
- The external heating during the occurrence of a low ambient temperature has a positive effect on reducing the temperature gradients between the centre and surface of the massive member. It is not appropriate to interrupt the heating process or to remove the tarpaulins too early, because it generates a reappearing increase in the temperature differences. It is especially important in the self-heating phase and during periods of extreme concrete temperatures.
- The measured histories of concrete temperature are highly consistent with FE results, which verifies the accuracy of the finite element model and confirms its practical usefulness for estimation thermal field in massive structure. The numerically identified temperature distribution gives the possibility to improve the composition of the concrete mixture before casting and helps to arrange locations of measuring sensors. Generally, thermocouples should be placed in the central part of structural element with the maximum permeability of the casting layer.
- In order to improve numerical predictions, it is recommended to use additional thermocuples to monitor the air temperature, the temperature at the interface between the concrete and the formwork or the styrofoam layer, and to conduct an independent measurement of the cooling wind speed.

CRediT authorship contribution statement

Aleksandra Kuryłowicz-Cudowska: Conceptualization, Methodology, Software, Visualization, Investigation, Data curation, Writing – original draft, Resources, Writing – review & editing, Project administration. **Krzysztof Wilde:** Conceptualization, Resources, Writing – review & editing, Supervision.

Declaration of Competing Interest

The authors declare that they have no known competing financial interests or personal relationships that could have appeared to influence the work reported in this paper.

Data availability

Data will be made available on request.

References

[1] J.H. Yeon, S. Choi, M.C. Won, In situ measurement of coefficient of thermal expansion in hardening concrete and its effect on thermal stress development, Constr. Build. Mater. 38 (2013) 306–315, https://doi.org/10.1016/j.conbuildmat.2012.07.111.
[2] B.A. Klemczak, Modeling thermal-shrinkage stresses in early age massive concrete structures – Comparative study of basic models, Archives of Civil and Mechanical Engineering 14 (2014) 721–733, https://doi.org/10.1016/j.acme.2014.01.002.
[3] M. Briffaut, F. Benboudjema, J.-M. Torrenti, G. Nahas, Effects of early-age thermal behaviour on damage risks in massive concrete structures, Eur. J. Environ. Civ. Eng. 16 (5) (2012) 589–605, https://doi.org/10.1080/19648189.2012.668016.
[4] B. Klemczak, A. Knoppik-Wróbel, Reinforced concrete tank walls and bridge abutments: Early-age behaviour, analytic approaches and numerical models, Eng. Struct. 84 (2015) 233–251, https://doi.org/10.1016/j.engstruct.2014.11.031.
[5] M. Batog, Z. Giergiczny, Influence of mass concrete constituents on its properties, Constr. Build. Mater. 146 (2017) 221–230, https://doi.org/10.1016/j.conbuildmat.2017.04.085.
[6] F. Lin, X. Song, X. Gu, B. Peng, L. Yang, Cracking analysis of massive concrete walls with cracking control techniques, Construct. Build. Mater. 31 (2012) 12–21, https://doi.org/10.1016/j.conbuildmat.2011.12.086.
[7] A. Smolana, B. Klemczak, M. Azenha, D. Schlicke, Experiences and analysis of the construction process of mass foundation slabs aimed at reducing the risk of early age cracks, Journal of Building Engineering 44 (2021), 102947, https://doi.org/10.1016/j.jobe.2021.102947.
[8] A. Smolana, B. Klemczak, M. Azenha, D. Schlicke, Early age cracking risk in a massive concrete foundation slab: Comparison of analytical and numerical prediction models with on-site measurements, Constr. Build. Mater. 301 (2021), 124135, https://doi.org/10.1016/j.conbuildmat.2021.124135.
[9] Y. Huang, G. Liu, S. Huang, R. Rao, C. Hu, Experimental and finite element investigations on the temperature field of a massive bridge pier caused by the hydration heat of concrete, Construct. Build. Mater. 192 (2018) 240–252, *https://doi.org/10.1016/j.conbuildmat.2018.10.128*.
[10] M. Kheradmand, M. Azenha, R. Vicente, J.L.B. de Aguiar, An innovative approach for temperature control of massive concrete structures at early ages based on post-cooling: Proof of concept, Journal of Building Engineering 102 (2020), 101832, https://doi.org/10.1016/j.jobe.2020.101832.
[11] S. Yehia, T. Landolsi, M. Hassan, M. Hallal, Monitoring of strain induced by heat of hydration, cyclic and dynamic loads in concrete structures using fiber-optics sensors, Measurement 52 (2014) 33–46, https://doi.org/10.1016/j.measurement.2014.02.030.
[12] J. Pan, W. Liu, J. Wang, F. Jin, F. Chi, A novel reconstruction method of temperature field for thermomechanical stress analysis of arch dams, Measurement 188 (2022), 110585, https://doi.org/10.1016/j.measurement.2021.110585.
[13] J. Zhang, F. Zheng, Z. Liu, S. Hong, B. Dong, F. Xing, Nondestructive monitoring on hydration behavior of cement pastes via the electrochemical impedance spectroscopy method, Measurement 185 (2021), 109884, https://doi.org/10.1016/j.measurement.2021.109884.
[14] A. Kuryłowicz-Cudowska, K. Wilde, J. Chróścielewski, Prediction of cast-in–place concrete strength of the extradosed bridge deck based on temperature monitoring and numerical simulations, Constr. Build. Mater. 254 (2020), 119224, https://doi.org/10.1016/j.conbuildmat.2020.119224.
[15] A. Kuryłowicz-Cudowska, Determination of thermophysical parameters involved in the numerical model to predict the temperature field of cast-in-place concrete bridge deck, Materials 12 (2019) 3089, https://doi.org/10.3390/ma12193089.
[16] A. Kuryłowicz-Cudowska, E. Haustein, Isothermal Calorimetry and Compressive Strength Tests of Mortar Specimens for Determination of Apparent Activation Energy, J. Mater. Civ. Eng. 33 (2021) 1–14, https://doi.org/10.1061/(ASCE)MT.1943-5533.0003634.
[17] A. Mariak, M. Kurpińska, K. Wilde, K. Wilde, M. Niedostatkiewicz, Maturity curve for estimating the in place strength of high performance concrete, MATEC Web Conf. 262 (2019) 06007.
[18] X.S. Huo, L.U. Wong, Experimental study of early-age behavior of high performance concrete deck slabs under different curing methods, Constr. Build. Mater. 20 (2006) 1049–1056, https://doi.org/10.1016/j.conbuildmat.2005.04.001.
[19] E. Haustein, A. Kuryłowicz- Cudowska, A. Łuczkiewicz, S. Fudala-Książek, B. M. Cieślik, Influence of Cement Replacement with Sewage Sludge Ash (SSA) on the Heat of Hydration of Cement Mortar, Materials 15 (2022) 1547, https://doi.org/10.3390/ma15041547.
[20] Q. Wang, M.X. Shi, D.Q. Wang, Contributions of fly ash and ground granulated blast-furnace slag to the early hydration heat of composite blinder at different

curing temperatures, Adv. Cem. Res. 28 (5) (2016) 320–327, https://doi.org/10.1680/jadcr.15.00077.
[21] E. Hernandez-Bautista, D.P. Bentz, S. Sandoval-Torres, P.F. De, J. Cano-Barrita, Numerical simulation of heat and mass transport during hydration of Portland cement mortar in semi-adiabatic and steam curing conditions, Cem. Concr. Comp. 69 (2016) 38–48, https://doi.org/10.1016/j.cemconcomp.2015.10.014.
[22] M. Cervera, R. Faria, J. Oliver, T. Prato, Numerical modelling of concrete curing, regarding hydration and temperature phenomena, Comput. Struct. 80 (2002) 1511–1521, https://doi.org/10.1016/S0045-7949(02)00104-9.
[23] J.E. Jonasson, P. Groth, H. Hedlund, Modelling of temperature and moisture field in concrete to study early age movements as a basis for stress analysis, International Symposium Thermal Cracking in Concrete at Early Ages, Munich (1994) 45–52.
[24] G. Di Luzio, G. Cusatis, Solidification–microprestress–microplane (SMM) theory for concrete at early age: Theory, validation and application, Int. J. Solids Struct. 50 (2013) 957–975, https://doi.org/10.1016/j.ijsolstr.2012.11.022.
[25] Z.P. Bažant, W. Thonguthai, Pore pressure and drying of concrete at high temperature, Journal of the Engineering Mechanics Division 104 (5) (1978) 1059–1079.
[26] C.E. Majorana, V. Salomoni, B.A. Schrefler, Hygrothermal and mechanical model of concrete at high temperature, Mater. Struct. 31 (6) (1998) 378–386.
[27] K.J. Bathe, Finite Element Procedures, Prentice Hall, 1982.
[28] J. Chróścielewski, J. Makowski, W. Pietraszkiewicz, Statyka i dynamika powłok wielopłatowych, Nieliniowa teoria i metoda elementów skończonych, Wydawnictwo Instytutu Podstawowych Problemów Techniki PAN, Warszawa, 2004 in Polish.
[29] Construction project „Wiadukt Biskupia Górka w Gdańsku. BPBK S.A., December 2015.
[30] CEN, EN 196-9 Methods of testing cement - Part 9: Heat of hydration - Semi-adiabatic method.
[31] Results of the hydration heat of CEM I 42,5 N HSR/NA, Institute of Ceramics and Building Materials, Kraków.
[32] Weather service, Institute of Meteorology and Water Management: http:/www.pogodynka.pl.
[33] https://pl.wikipedia.org/wiki/Wiadukt_Biskupia_Górka.
[34] Project of composition of concrete, C30/37 class.
[35] EN-1992-1-1:2008. Eurocode 2: Design of concrete structures - Part 1-1: General rules and rules for buildings.
[36] K. Breugel, Artificial cooling of hardening concrete, Delft University of Technology, Delft, Concrete Structures, 1980.
[37] P. Lura, K. Breugel, Thermal Properties of Concrete: Sensitivity Studies, IPACS Document, Subtask 2 (2001) 5.
[38] S. H. Kosmatka, B. Kerkhoff, W. C. Panarese, Design and Control of Concrete Mixtures, 14th Edition, Portland Cement Association, Skokie, Ill., 2003, pp. 323-325.
[39] K.A. Riding, J.L. Poole, A.K. Schindler, M.C.G. Juenger, K. j., Folliard Evaluation of Temperature Prediction Methods for Mass Concrete Members, ACI Mater. J. 103 (5) (2006) 357–365.
[40] EN 13670, Execution of concrete structures, CEN (European Committee for Standardization), Brussels, Belgium, 2010.